Advanced Ultrasonic Inspection of Thick-Section Composite Structures for In-Field Asset Maintenance

Citation for published version:
Quinn, JA, Davidson, J, Bajpai, A, Ó Brádaigh, CM & McCarthy, E 2023, 'Advanced Ultrasonic Inspection of Thick-Section Composite Structures for In-Field Asset Maintenance', *Polymers*, vol. 15, no. 15, 3175. https://doi.org/10.3390/polym15153175

Digital Object Identifier (DOI):
10.3390/polym15153175

Published In:
Polymers

Article

Advanced Ultrasonic Inspection of Thick-Section Composite Structures for In-Field Asset Maintenance

James A. Quinn *, James R. Davidson, Ankur Bajpai, Conchúr M. Ó Brádaigh and Edward D. McCarthy

School of Engineering, Institute for Materials and Processes, The University of Edinburgh, UK
* Correspondence: J.Quinn@ed.ac.uk

Abstract: An investigation into the inspection capabilities of in-field advanced-ultrasound detection, for use on ultra-thick (20 to 100 mm) glass fibre-reinforced polyester composites, is presented. Plates were manufactured using custom moulding techniques, such that delamination flaws were created at calibrated depths. Full matrix capture with an on-board total focussing method was used to detect flaws scanned by a 0.5 MHz linear array probe. Flaw through-thickness dimensions were altered to assess the threshold for crack face separation at which delaminations could be identified. Furthermore, part thickness and in-plane flaw dimensions were varied, to identify the inspection capability limitations of advanced-ultrasonics for thick composites. Results presented in this study demonstrate an inverse relationship between ability to find delaminations and plate thickness, with inspection successful at depths up to 74 mm. When delamination thickness exhibit surface-to-surface contact, inspection capability reduced to 35 mm. Exponential decay relationships were observed between the accuracy of flaw depth measurement and plate thickness, deemed an artefact of the requirement for low probe frequencies. Effective inspection depth was determined to be in the range of 1 to 20 times wavelength. It is speculated that the accuracy of measurement could be improved using probes having novel coupling solutions, and detectors having optimised signal processing/filtration algorithms.

Keywords: Non-destructive testing; Ultrasonics; Delamination; Full matrix capture

1. Introduction

Non-destructive testing (NDT) is the term given to techniques which assess component integrity without inducing material damage. For asset maintenance, NDT techniques have been incorporated into established operational programmes to evaluate component performance throughout the service life period. Current examples include fleet maintenance operations by the Royal National Lifeboat Institution (RNLI) [1,2] and routine Ultrasonic Testing (UT) of fibre-reinforced polymer (FRP) structures—such as train carriages, minehunters and submarines—by Babcock International Group plc [3,4]. NDT of composite materials is a well established field, and has been comprehensively explored in several literature reviews (for example, in references [5–7]) and optimised (for example, in references [8–10]). However, the majority of publications focus on thin laminate structures (up to 15 mm thick) commonly found in the aerospace and aeronautical industries. In wind/tidal turbine blades, military vehicles, ships, and other sea-going vessels, structures are often primarily constructed from monolithic FRPs exceeding 20 mm thickness—some of which have been in service for several decades [11–13]. A brief summary of research studies relevant to thick-section composite UT is provided as follows.

Ultrasonic testing is a popular NDT technique in which the propagation of ultrasonic waves (typically short pulse waves with centre frequency in the range of 0.1 to 15 MHz) within a material subject, is observed [14]. For example, features such as cracks [15–18], delaminations [19–22], variations in structural and material constitution [23–26] and manufacturing defects [27–30] may present as changes in the transmission and reflection energy or changes in the phase of return signals [31]. The term "advanced" when

Citation: Lastname, F.; Lastname, F.; Lastname, F. Title. *Journal Not Specified* **2023**, *1*, 0. https://doi.org/

Received:
Revised:
Accepted:
Published:

applied to ultrasonics has become broadly accepted in the field to describe a subset of ultrasonic equipment and methods that utilise computerised data collection and processing [32]. Some (non-exhaustive) examples include Phased Array UT (PAUT) , Time of Flight Diffraction (TOFD), Automated Ultrasonic Testing (AUT) and Total Focussing Method (TFM) [33–37]. Equipment and methods that fall outwith these groupings (such as pulse-echo A-scan UT) are occasionally termed "conventional", for example, as in references [38–41]. Ultrasonic inspection of composite materials is a complex activity, where subject constitution (for example, the fibre volume fraction and/or alignment of anisotropic plies), must be considered. Such variations in the original quality of a composite part will change the material response when subjected to UT, for example, increased porosity will alter the dispersion and bulk velocity properties [42,43]. Furthermore, each component of the composite system will have different acoustic properties (for example, attenuation and wave propagation velocity), and therefore differences in fibre volume fraction between specimens (either as a global parameter or locally e.g. in the form of resin-rich zones) will bias the global specimen acoustic properties towards those of the more dominant phase [44]. The UT of thick composites presents the particular challenge of requiring the low attenuation and greater penetration ability of smaller inspection frequencies (often ≤ 1 MHz) due to the usually high damping properties of polymeric materials. However, these low frequencies typically result in reduced spatial resolution [45–47].

The NDT of marine composite structures was investigated by Mouritz et al [48], where a Krautkramer-Branson USD15 flaw detector (paired with a Panametrics 0.5 MHz transducer probe) was used to perform pulse-echo A-scan inspection for artificial delamination-style flaws embedded in polyester-glass panels. Test specimens ranged from 25 to 150 mm in thickness, and polytetrafluoroethylene (PTFE) film was used to embed flaws of different in-plane dimensions at various depths. Detectable flaws were consistent with damage observed as result of high-cycle fatigue stresses, such as small (approximately 10 mm) in-plane delaminations, at depths up to 100 mm. Research outcomes from Mouritz et al provide ideal benchmarks for analysing the performance of pulse-echo A-scan UT with thick FRPs, especially for the thicknesses typically utilised in the marine sector. Nevertheless, these are somewhat dated, given the continual development of "advanced" ultrasonic equipment including detectors, probes, and sophisticated softwares/analysis tools [49,50].

Subsequently, Battley et al [51] completed an evaluation of NDT for inspecting marine composites, and considered techniques such as UT, tap-testing, and microwave testing. Inspected materials were divided into two categories: real marine structures with pre-existing damage, and manufactured parts with calibrated damage. Sandwich structures with various skin and core thicknesses were predominantly considered, although several monolithic glass-FRPs were also evaluated. Instances of the former are listed as follows: glass fibre/epoxy skin with foam core, glass fibre/epoxy skin with balsa core, carbon fibre/epoxy (prepreg) skin with honeycomb core, gelcoat/glass FRP/plywood skin with balsa core, and glass FRP/Kevlar skin with foam core. Calibrated delaminations were introduced by embedding PTFE film during laying-up, whilst voids were simulated using heat-sealed polyethylene bags containing dry fibreglass cloth. Both types of defect were introduced in four different dimensions and at three unique depths. Notably, UT and microwave testing were able to detect deep flaws in glass FRP up to 16.6 mm thick, whilst tap-testing was deemed unsuitable. UT was incompatible with rougher surfaces, which could potentially restrict wider uptake in marine applications—where course inspection surfaces are common.

A conventional through-thickness UT immersion system was utilised by Balasubramaniam and Whitney [52] in 1996, to characterise the elastic stiffness properties of thick-section glass FRPs. In this study, the descriptor "thick" corresponded to part thicknesses which were greater than ten times the wavelength of the scanning wave—in this case up to 28 mm. Utilising pairs of 0.5 and 1.0 MHz transducers, a numerical method was used to find the stiffness of inspected composites wherein peak location and time of flight data were used to calculate phase angle and (non-dispersive wave) phase velocity. When compared to conventional methods, measurement errors of the UT technique were observed to be 5-7 %. Whilst the examined through-thickness attenuation or immersion techniques have limited applicability in large structures, since both sides of the component may not be accessible, the value of estimating mechanical properties using UT is evident, and the definition of thick composites as a function of wavelength is important for unifying terminology in the proceeding literature.

More recently, Ibrahim has published comprehensive reviews of NDT of thick section composites [53,54], suggesting that UT of thick section composites is immature compared to that of metallic structures, and that NDT techniques are incapable (circa 2016) of full and complete inspection of composite structures. In an article by Taheri and Hassen (2019) [5], the comparative advantages of phased array UT were evaluated for the inspection of glass FRP composites up to 25 mm thick. Finite depth holes of varying diameter were drilled into one side of the panels, and both single element UT (0.5, 1.0 and 1.5 MHz) and array UT (1.5 MHz wedge transducer) were used to inspect from the opposing side. Signal-to-noise ratios were used to evaluate the suitability of each technique, with advanced UT exhibiting 15 % increases over conventional UT. As such, the authors concluded that advanced UT detects defects as small as 0.7 mm in diameter; a significant improvement over conventional UT. However, the study by Taheri et al is restricted to 25 mm thicknesses; further research is required to determine efficacy when structures exceed approximately 25 mm, such as in marine and renewable applications.

A practical assessment of the applicability of various NDT methods for assessing damage in composite structures was compiled by Sheppard et al [55]. Tap testing, shearography, radiography, microwave testing, thermography, and phased array UT were considered for marine sub-assemblies, consisting of 12 mm thick monolithic glass FRP laminates bonded to structural reinforcement hats. The latter were constructed from non-structural foam with structural polyvinyl chloride cores, and skinned with vacuum-bag cured carbon fibre plies. Phased array UT was performed using a Rapidscan 2 system, consisting of a 2 MHz, 64 element, water-filled rubber wheel probe. The resulting A-scans were difficult to interpret, with area coverage being time-consuming due to the small probe contact area. Nonetheless, voids, defects, and inclusions were detectable in the parts, and additional detection in the structural hats on the reverse side was also possible; thus, dis-bonding of the structural hats from the monolithic body observable. The progress towards advanced ultrasonics with thick FRPs provides opportunity for detecting flaws with greater accuracy, including potential for more effective signal filtering to combat the issues of scattering and deflection encountered when scanning composites. Despite these equipment advantages over the research previously discussed, Sheppard et al only consider maximum FRP thickness of 12 mm, as is typically found in lifeboats, yachts and pleasurecraft; further research is required to determine efficacy in thicker structures.

Given the current lack of published research, the present study provides a critical analysis of in-field advanced UT of existing thick and ultra-thick monolithic FRPs. The findings contribute towards alleviating premature disposal/decommissioning of large composite components, which is of particular importance given recent concerns regarding sustainability and end-of-life solutions for composite and polymeric materials [56–59].

2. Materials and Methods

2.1. Materials

The material system and manufacturing methods used in the present work were selected to represent that of typical marine composite structures. Crystic 489PA isophthalic polyester resin and (2 % by volume) Butanox M50 methyl ethyl ketone peroxide crosslinking initiator, were combined and subsequently impregnated into the reinforcing fibres. The reinforcement was 800 g m^{-2} plain woven glass mat, supplemented where necessary with 300 g m^{-2} chopped strand glass mat—to compensate for accumulation of crimp and to maintain consistent plate thickness. The curing cycle was 24 h at room temperature (20 °C) with no additional environmental control or post-curing steps.

2.2. Manufacturing

Five variations of glass FRP plate were manufactured, where the panel thickness was increased from 20 to 100 mm, at fixed intervals of 20 mm. The fabrication process consisted of placing fibre mats warp-on-warp, and impregnating the resin mix using a combination of brushes, plastic wedges, and rollers. The fibre volume fraction (V_r) was controlled in each ply by evenly distributing the liquid resin until a fibre volume fraction of approximately 45 % was reached—calculated using Equation 1 (transcribed from ASTM D3171-15) where: M_r is the mass ratio of reinforcement in the ply, ρ_c is the density of the cured composite (1.9 g cm^{-3}), and ρ_r is the density of the reinforcement. Artificial cavities which acted as simulated flaws were created at strategically selected depths—relative to the total thickness—for each panel, as shown in Table 1. The intention of these artificially generated flaw cavities was to simulate in-plane delaminations which may be developed as a consequence of accumulated in-service damage in real structures. Detection of out-of-plane flaws and/or manufacturing-derived defects remains an equally important task, however the in-plane dimensions of these types of features are often much smaller, resulting in a different set of challenges for successful NDT, compared to the scope of the present work. Cavity locations were selected to generate a full range of— absolute and relative—cavity depths whilst including some relative cavity depths in multiple plates. The process of producing artificial cavities in plates is represented schematically in Figure 1. Cavity formation required the lay-up process to be paused at predefined part thicknesses. After the resin was fully hardened, a series of rotary tools and manual files were used to recess a 3 mm deep stepped shape into the (current) top surface of the part. Steel male counterparts, machined in the same stepwise pattern and coated with Loctite Frekote NC770 mould release agent, were then placed into the recesses. The lay-up was resumed until the next target depth was achieved, or until plate completion. Upon completion of final curing, the steel tools were removed from the plates, resulting in geometrically consistent cavities. A small draft angle was filed into all sharp edges of the steel tools such that a nylon-headed hammer could be used to lightly tap the tools out with ease. For all plates, precise geometry diagrams (showing all cavity locations/depths) are given in Figure 2.

$$V_r = (M_r) \times 100 \times (\rho_c/\rho_r) \tag{1}$$

Table 1. Flaw depth locations relative to plate thickness.

Plate	Depth from front face			Depth from rear face			V_r (%)	
Thickness	Flaw 1	Flaw 2	Flaw 3	Flaw 1	Flaw 2	Flaw 3	Mean	SD
20 mm	25 %	50 %		60 %	35 %		44.7	8.5
40 mm	12 %	25 %	50 %	80 %	68 %	43 %	44.4	8.3
60 mm	8 %	25 %	50 %	86 %	70 %	45 %	40.4	8.3
80 mm	6 %	25 %	50 %	90 %	71 %	46 %	41.9	11.0
100 mm	10 %	20 %	30 %	77 %	67 %	57 %	46.4	13.8

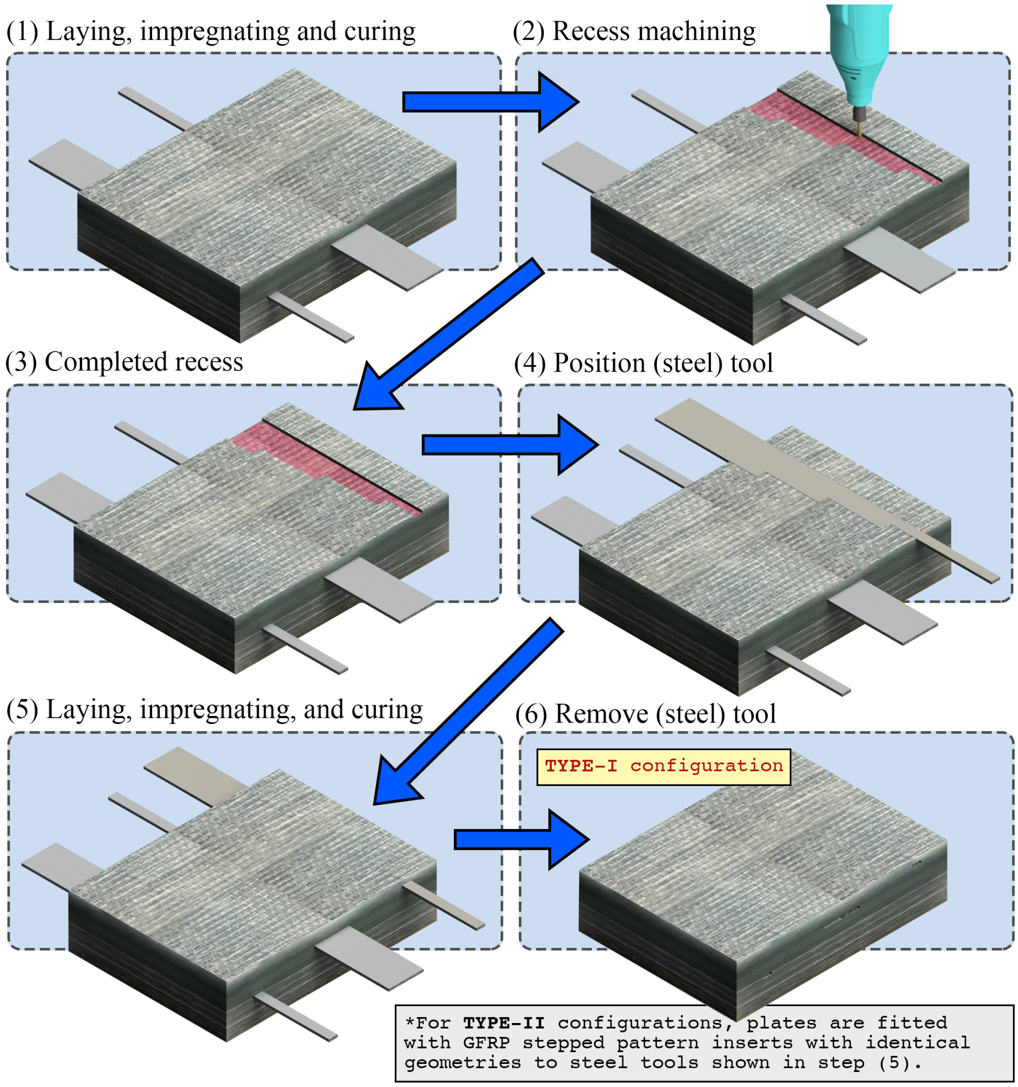

Figure 1. Schematic diagram of manufacturing process.

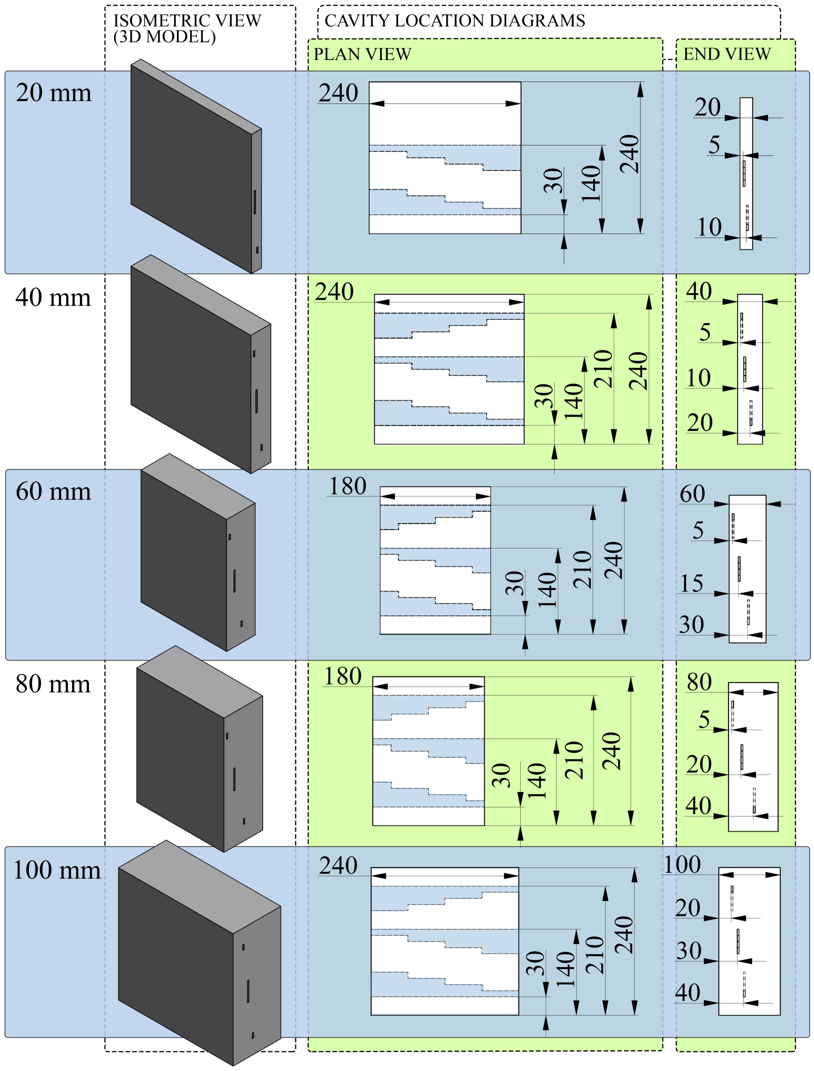

Figure 2. Plate geometry and cavity location diagrams (all dimensions in mm).

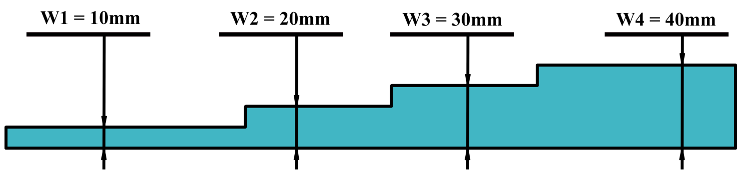

Figure 3. Schematic of cavity stepwise pattern including width dimensions.

Three stepped pattern inserts, with identical shapes to that of the steel moulds, were manufactured by hand lay-up of the same glass FRP system. The in-plane geometry of the glass FRP inserts was machined until a hole-based transition fit (designated 3n14 in ISO 286-1:2010) was achieved—based on sliding inserts within the plate cavities. By utilising glass FRP inserts, the effect of cavity size could be explored as an independent variable, with two possible values: no glass FRP insert (3 mm deep cavities), denoted Type I; and 4-ply glass FRP insert (all-over fixed-transition engineering fit), denoted Type II. The former acted as a reference case in which UT should be capable of detecting the defects as indicated by existing literature, while the latter simulated delaminations which have surface-to-surface contact—potentially as a result of interlaminar shear exhibit after crack formation—without the inclusion of foreign materials such as PTFE.

2.3. Testing

2.3.1. Equipment Description

Inspection of calibrated flaws was performed using a Sonatest Veo+ advanced ultrasonic detector paired with a Sonatest X6B-0.5M64E-2x10 (64 elements, 0.5 MHz) linear array probe. The 0.5 MHz probe used was the lowest frequency stock array probe offered by the original equipment manufacturer in the commercial market, and was selected to ensure the greatest possible penetration depth in order to obtain strong backwall signatures, at the expense of greater resolution. Similar inspection frequencies ($\leq$1 MHz) have been previously used to complete inspections on FRP of similar thicknesses, for example, in references [5,48,52]. Given the comparatively large penetration depth required for this use case (100 mm), relative to typical composite ultrasonic inspections, this compromise was considered favourable. An on-board full matrix capture total focusing method (FMC-TFM) was selected, as this approach completes full time of flight calculation for every focal point and transmitter-receiver combination, thereby exhibiting improved resolution over traditional phased array scanning. A regular cuboidal probe wedge measuring $25 \times 50 \times 130$ mm—cast from optical-grade acyrlic and coated with a thin film of coupling agent—provided further noise filtration. The coupling agent utilised was a 1:1 (ratio) mixture of Sonagel Utrasonic Couplant and tap water. A linear encoder calibrated to 16 ticks/mm was used in the scan axis, such that linear sections (denoted as sectors) of the specimens could be displayed in both B-scan and C-scan arrangements.

2.3.2. Data Acquisition

Two discrete plate scanning configurations were considered in this work: (I) plates with no inserts, and (II) plates fitted with glass FRP inserts. The scanning procedure—to be described in the present section—was applied to both cases.

Specimens were lightly scrubbed with an acetone towel and placed face up on a clean table top. The probe scan width was set to 30 mm, in accordance with manufacturer recommendations based on providing an effective focus. Calibration of the detector settings (velocity, gate positioning) was performed using a reference block of the same GRP system, which contained no damage or delaminations, such that the gates were positioned between the front and back wall echos and depth measurements were scaled appropriately. Each specimen was divided into 30 mm wide strips (sectors) on the inspected face using a marker, with each sector numbered sequentially (Figure 4a) to ensure full scan coverage of the specimen. Immediately prior to initial scanning on each specimen, a calibration procedure was first performed. This consisted of ensuring the detector was programmed with the correct target thickness and appropriate gain values, to maximise feature visibility relative to noise. Due to working memory limitations of the detector in TFM mode, the on-board scan depth was set to half of the part thickness when exceeding 60 mm thick, and affected specimens were scanned twice at each sector—firstly for the (depth-wise) top half and followed by the (depth-wise) lower half. No further adjustments were applied to the on-board scan settings, on the basis of attempting to replicate real-world use cases where set-up is based on part geometry (thickness, coreners, radii etc) and material acoustic properties. This is particularly important since the existence, dimensions, positioning, and depth of flaws/damage are unknown in real-world applications. At the end of each sector, data for A-scans, B-scans, and C-scans were saved and exported for post-processing. This process was repeated for both faces of the plate, thereby doubling the quantity of depth measurements for each cavity.

2.3.3. Post-processing

Ultrasound scan data was exported from the detector in the form of native .utdata files, which store the entire data set (A, B and C-scans) for the given encoded region. These files were post-processed in Sonatest UTStudio+ software where colourmap and software gain were adjusted to output image files of representative A, B and C-scans. The C-scans sectors for each specimen were stitched together using GIMP 2.10.4, effectively creating raster/mapped scans. Determination of whether a delamination feature could be identified during the scanning was completed primarily with data from B-scans; the identification of delaminations were noted both in terms of feature depth and signal amplitude relative to noise in corresponding A-scans. Depth measurements were obtained using gate positioning to ensure consistency across the data set, whilst in-plane dimensioning was measured as the linear distance travelled by the probe on the plate outer face while the flaw signal amplitude remained above the ambient noise gate.

3. Results and Discussion

3.1. Representative Scans

The first specimen (20 mm thick with Type I flaws) is presented as a case study in Figure 4, showing the scanning methodology (Figure 4a), followed by the corresponding C-scan for each encoded sector (Figure 4b). Sector 3 of that specimen was chosen to display a representative encoded B-scan (Figure 4c), and the corresponding A-scans when the probe was placed directly above each flaw are included in Figures 4d-4e. Uncategorised variations in acoustic impedance—experimental noise—were observed in some specimens, characterised by high-amplitude peaks in A-scans and subsequent low signal return regions in B- and C-scans, shown in Figure 5. To verify the status of peaks at these locations as noise rather than delaminations, sections of the affected plates were extracted using a diamond-bladed wet saw, polished, and examined using a Zwiss Axioskop2 microscope (Figure 6, X-Z plane view). Regions where unexpected variations in impedance were observed corresponded to plies consisting of short reinforcement fibres, increased void content (for example, air bubbles), and less homogeneous resin dispersion, relative to areas of the plate where typical ultrasound response was observed. Specimens were manually delaminated at this region to observe the X-Y (in-plane) view of the plies which were revealed as chopped strand mat plies. By contrast, randomly selected plies were delaminated from the remainder of the specimen and were observed as woven roving mat plies. The amplitude of waveform returned from a chopped strand mat region can resemble that from a delamination, particularly when the former is closer to the probe than the latter (Figure 5). It may be possible to distinguish between causes of impedance gradients by monitoring signal response waveforms on-board during inspection, however, some modern UT detectors may not have this functionality.

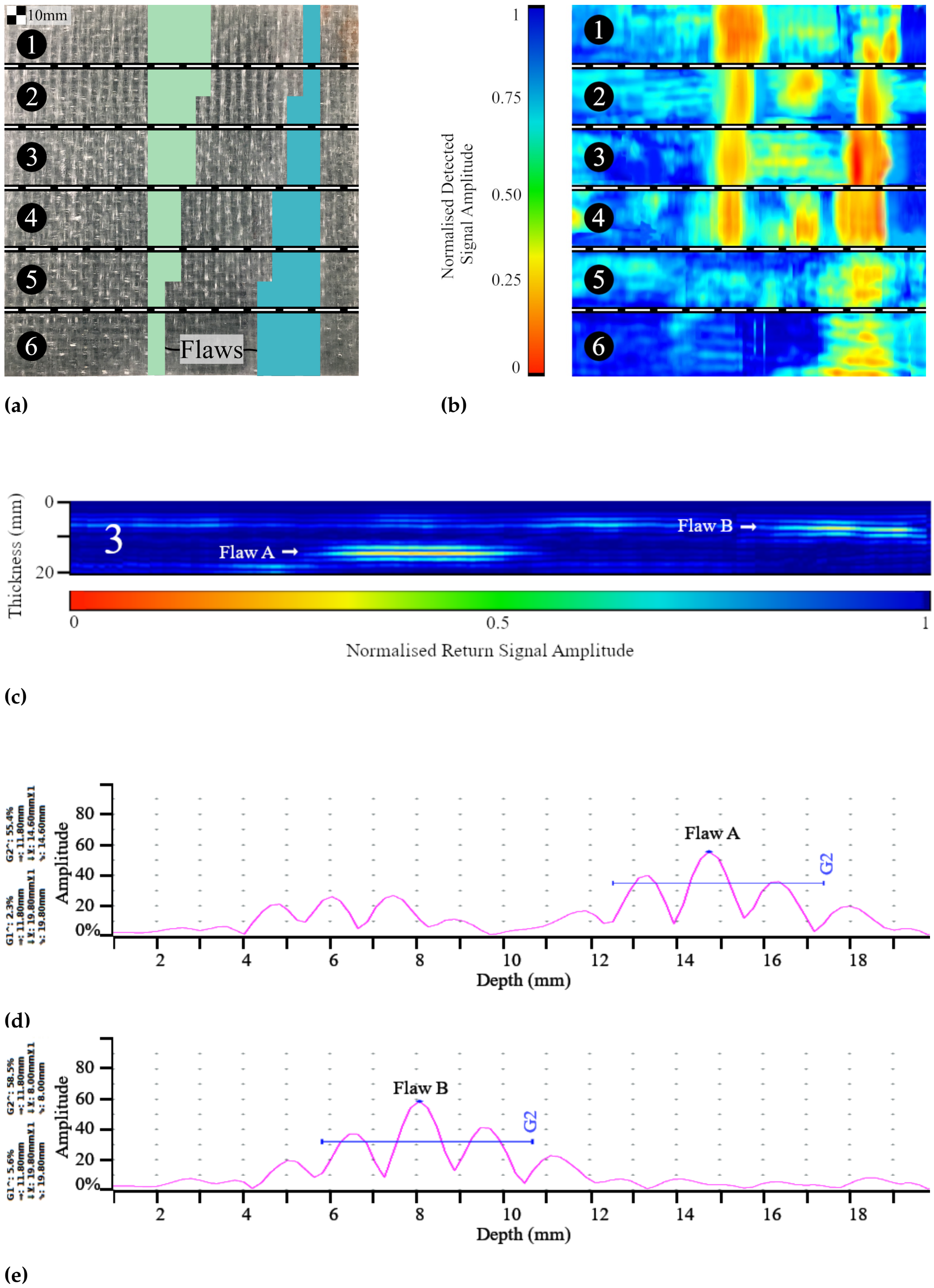

Figure 4. Scanning procedure for representative 20 mm plate: (a) Sector locations. (b) C-scans. (c): Sector 3, B-scan. (d) A-scan at Sector 3, Flaw A. (e) A-scan at Sector 3, Flaw B.

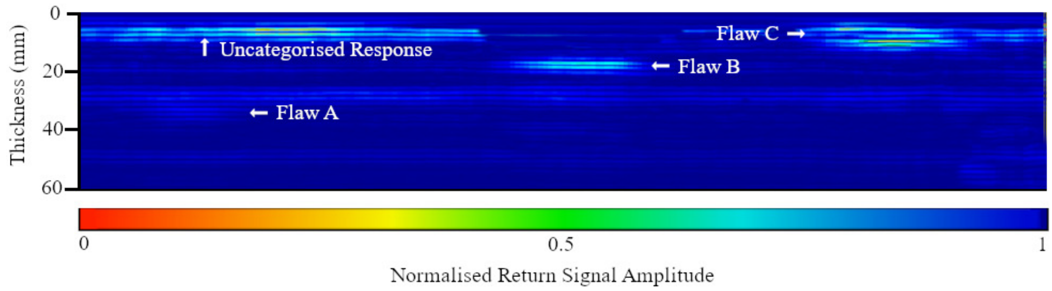

Figure 5. Representative B-scan of the 60 mm specimen.

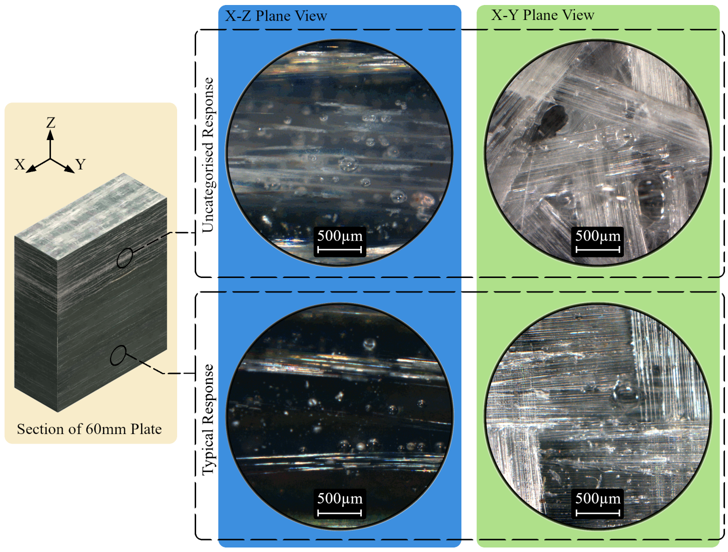

Figure 6. Microscopic examination of scan features in a section cut from the 60 mm specimen.

Furthermore, in-field asset inspection is routinely performed on parts of unknown structural condition; the ability to detect acoustic features without determining causation could lead to misjudgement of an inherent acoustic feature (for example, a resin rich zone or chopped strand mat region) as a crack, delamination, dis-bond, or other structural damage. It is therefore possible for an benign acoustic feature to obscure a damage region, for example, Flaws A and B in Figure 5 are Type I delaminations (3 mm thick) and are easy to overlook during inspection due to the masking effect of the—previously uncategorised—chopped strand mat/experimental noise region.

3.2. Plate Thickness

The ability to find flaws was assessed by comparing the percentage of flaws found as a function of plate depth (Figure 7). The percentage of flaws observed was herein defined as the ratio of number of flaws which could be seen, to the total number of flaws in a given plate.

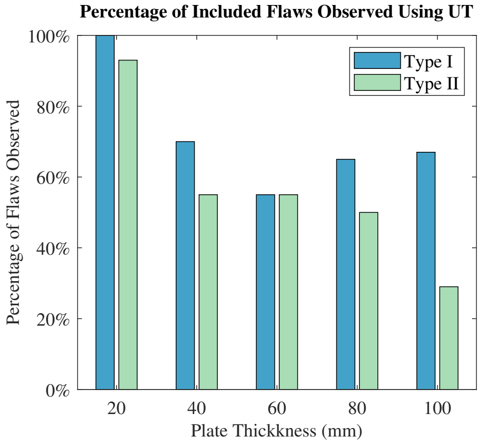

Figure 7. Observability of flaws using UT (Type I and Type II).

For both Type I and Type II flaws, increasing plate thickness is correlated with a general reduction in percentage of flaws found, for example; in the 20 mm thick plate, 100 % of the Type I flaws and 93 % of the Type II flaws were identified. This reduces to 66 % and 29 % respectively for the 100 mm thick plate. The relationship between part thickness and ability to find flaws is expected since the composite is constructed from two materials which have different acoustic properties—glass and polyester—hence increasing the ply count through thickness creates more boundaries where the ultrasound waves refract. The drop in observation of Type I flaws in the 60 mm thick plate is caused by particularly large peak responses from CSM regions in that plate, which were often positioned between the detector and the flaw, and made observation of the calibrated flaw peaks challenging—it is anticipated that without the presence of these CSM plies, more Type I flaws would have been observed. Furthermore, for the ultrasound signal to penetrate into a composite at the thicknesses in the present work necessitates ultra-low frequencies, which reduce sensitivity while increasing attenuation and beam spread [60]. Where flaws are small relative to part thickness (Type II), these factors combine to cause significant drop-off in detection capability, especially as the plate thickness increases. As a direct consequence of the above factors, presently there is strong possibility of delamination style flaws in composite laminates greater than 20 mm thick remaining undetectable with present in-field UT technologies—especially where the delaminated crack faces are in contact—independent of the inclusion or positioning of CSM plies.

3.3. Flaw Depth

The present work included a range of real flaw depths, defined as the distance between the external face of the flaw and the probed face (measured with Vernier Calipers). The percentage difference between the flaw depth measured by UT and the real depth is shown in Figure 8a as a function of real, absolute flaw depth. Similarly, the depth difference of the UT measurement as a function of relative flaw depth is shown in Figure 8b, where relative flaw depth corresponds to the ratio of real flaw depth to plate thickness. A Least Squares Optimisation method was used to fit exponential decay function (EDF) trend-lines to the data shown in Figure 8, the function of which is shown in Equation 2, with the parameters A and B listed in Table 2. In order to further probe depth measurement accuracy as a function of plate thickness, the results for all plates are re-plotted in Figure (9).

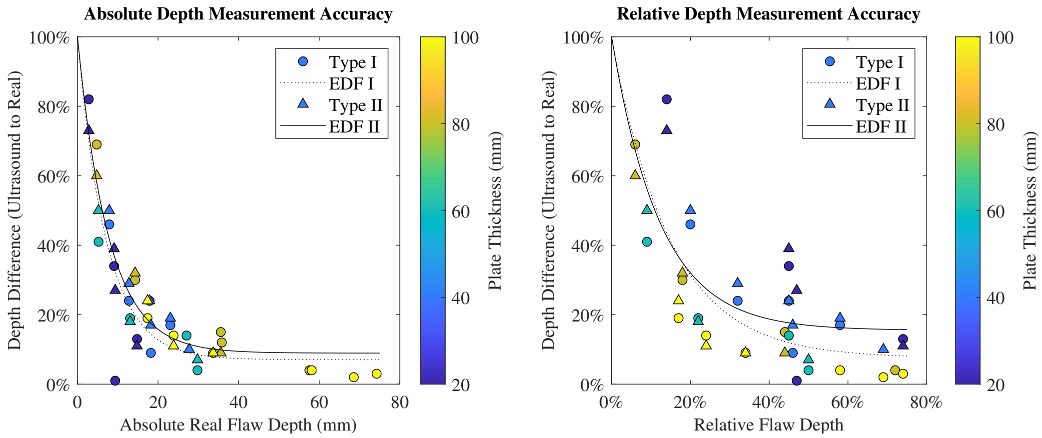

(a) **(b)**

Figure 8. Overall flaw depth measurement: (a) Percentage difference between flaw depth measured using UT and real flaw depth as a function of plate thickness, for both Type I and Type II flaws.(b) Percentage difference between flaw depth measured using UT and real flaw depth as a function of plate thickness, for both Type I and Type II flaws.

$$f(x) = (1 - \mathrm{B})\exp\left(\frac{-x}{\mathrm{A}+\mathrm{B}}\right) \tag{2}$$

Table 2. EDF trend-line parameters for Figure 8.

Figure	Flaw	A	B
6a	Type I	7.18	0.07
	Type II	7.73	0.09
6b	Type I	0.14	0.08
	Type II	0.12	0.15

Figure 8a demonstrates an inverse relationship between real flaw depth and the accuracy of the flaw depth measurement by UT, for both Type I and Type II flaws. The average percentage difference between UT depth measurement and real depth was 22 % for Type I and 27 % for Type II. The maximum depth at which a flaw could be identified was 74 mm for Type I and 35 mm for Type II. Flaw depth relative to plate thickness is shown in Figure 8b. Irrespective of plate thickness, no flaw can be seen beyond approximately 74 % relative thickness, holding for both Type I and Type II flaws.

Some relative flaw depths (such as 45 %) were included in several plates, resulting in a range of data points captured at those relative depths. Colorbar scales were used in Figure 9a (Type I) and Figure 9b (Type II) to highlight the accuracy of depth measurements as a function of plate thickness where the range of relative depths is clearly displayed. For similar relative depths, further analysis (Figure 9) again shows reduced measurement accuracy when scanning less-thick plates (for both Type I and Type II flaws), further reinforcing the inference of an inverse relationship between plate thickness and flaw depth measurement accuracy. The necessity of low-frequency probes to attain signal penetration when inspecting thick composites is well established, and it is speculated that this is—in part—responsible for the reduction in measurement accuracy at shallow flaw depths. In the present work, all of the inspection was in the in the range of 1 to 20 times sound wavelength (the latter being approximately 5 cm), therefore, the waves may not have had the physical distance necessary to develop fully. Furthermore, it is possible that on-board filtration algorithms are better equipped to distinguish between noise and real features when the cavities are at greater depths, owing to a multitude of factors including noise attenuation and signal-to-noise ratio. When considering less thick plates, no general trend was observed between type of flaw and measurement accuracy, however, in thicker plates (above 60 mm or 45 % relative), the depth measurement of Type I flaws is more accurate than that of Type II flaws. Furthermore, at these plate thicknesses, the percentage of Type II flaws that could be inspected drops significantly compared to Type I (Figure 7).

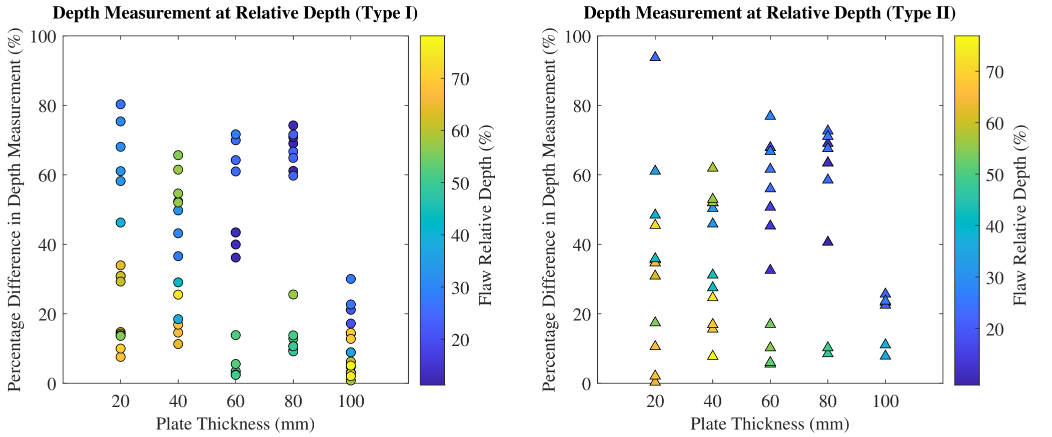

(a) **(b)**

Figure 9. Percentage difference of all observable flaw depth measurements as a function of plate thickness: (a) Type I flaws (b) Type II flaws.

3.4. In-Plane Flaw Dimensioning

In-plane flaw dimension analysis was completed to evaluate the accuracy of UT as a method for determining the size of a delamination style flaw in the lamina plane. Figure 10 shows the absolute measured flaw width as a function of plate thickness, whilst Figure 11 displays the accuracy of the width measurement by UT as a function of flaw depth. The accuracy of width dimensioning was defined as the percentage difference between the UT measurement and the known actual flaw width.

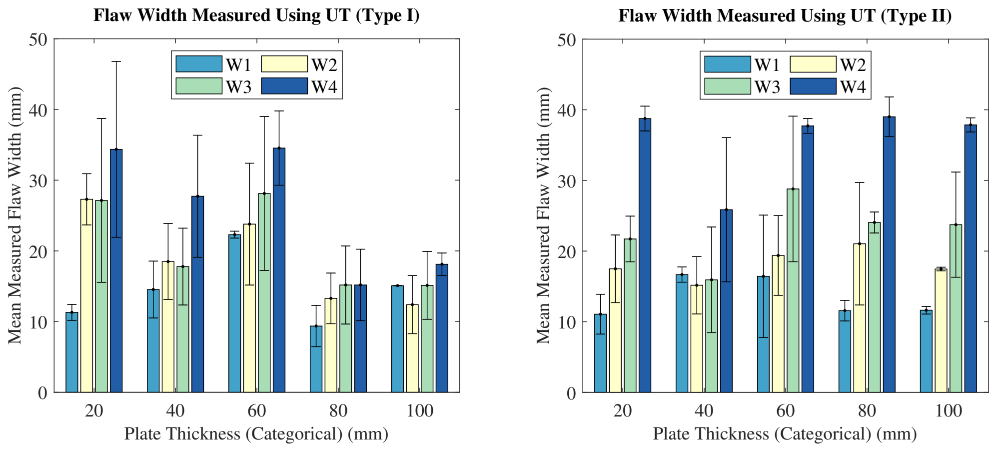

(a) **(b)**

Figure 10. Average UT-measured flaw widths (with standard deviations) at each known flaw width, as a function of plate thickness: (a) Type I flaws. (b) Type II flaws.

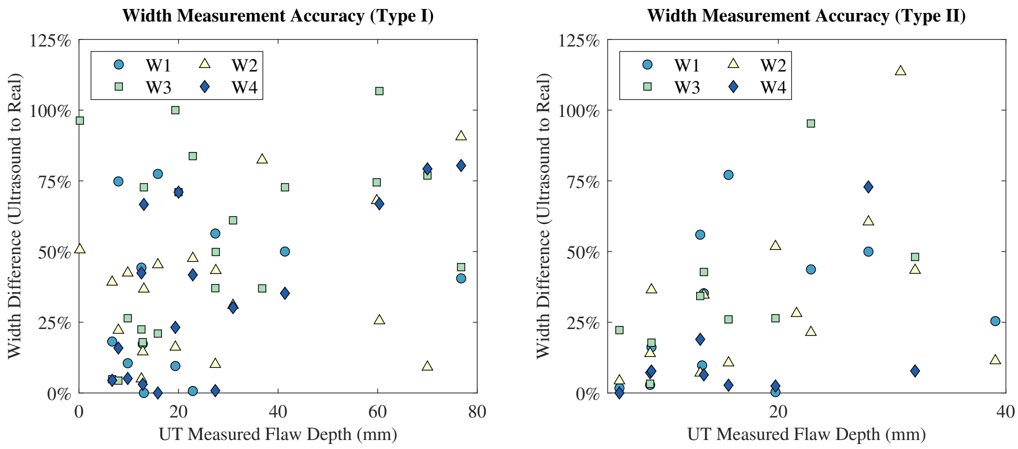

(a) **(b)**

Figure 11. Percentage difference between UT-measured flaw widths and known, actual flaw widths as a function of UT-measured flaw depth: (a) Type I flaws. (b) Type II flaws.

Examining Figure 10, no trend exists between UT-measured flaw width and plate thickness, for both flaw types. The standard deviations of width measurements have much variance across the test matrix, reinforcing the general inaccuracy of the technique for in-plane dimensioning. Furthermore, the analysis of width measurement accuracy in Figure 11 displays lack of relationship between in-plane measurement accuracy and flaw depth. Generally, Type II flaws were more accurately measured than Type I flaws, however, there is no statistical significance. Additionally, there were less Type II flaws identified than Type I, especially at larger plate thicknesses, therefore the direct comparison of Type I and Type II is ill-advised in this respect.

4. Conclusion

The efficacy of in-field advanced ultrasound to detect delamination flaws in thick section composites was evaluated using a full matrix capture total focusing method. A range of delaminations were generated during manufacturing of glass reinforced polymer blocks which ranged in total specimen thickness from 20 to 100 mm, whilst thickness, in-plane dimensions, and depth location were selected as flaw variables. In the present work (ie for this material system, specimen construction and UT system), 3 mm thick flaws are identifiable when embedded at depths up to 74 mm, reducing to 36 mm for surface to surface contact delaminations. Regardless of thickness, flaws were observed when embedded at depths up to 74 % of plate thickness, beyond which signal decay, noise and mechanically-benign acoustic features limited the success of industrially-representative inspection methods. Inverse relationships were observed between specimen thickness and flaw detection, as well as accuracy of flaw depth measurement and depth of flaw. No trends were observed when evaluating capability to dimension flaws in-plane, regardless of delamination size or specimen thickness. Consequently, this advanced ultrasonic inspection system with total focusing methods is effective for detecting delaminations in thick composites (up to 100 mm), provided the flaw is located at no greater than 74 % of part depth. However, deeper-set flaws and smaller damage cavities can remain undetected. Furthermore, any feature in the composite which generates a gradient of acoustic impedance with the bulk of the composite (such as a new fibre reinforcement or a resin-rich zone) could be readily misinterpreted as a region of delamination or disbonding.

Author Contributions: Conceptualization, James A. Quinn.; methodology, James A. Quinn.; formal analysis, James A. Quinn; investigation,James A. Quinn and James R. Davidson; resources, James A. Quinn.; data curation, James A. Quinn.; writing—original draft preparation, James A. Quinn, James R. Davidson, Ankur Bajpai; writing—review and editing, James A. Quinn, James R. Davidson, Ankur Bajpai, Edward D. McCarthy and Conchúr M. Ó Brádaigh; visualization, James A. Quinn and James R. Davidson; supervision, Edward D. McCarthy and Conchúr M. Ó Brádaigh.; project administration,

James A. Quinn and Edward D. McCarthy.; funding acquisition, Edward D. McCarthy and Conchúr M. Ó Brádaigh. All authors have read and agreed to the published version of the manuscript.

Funding: This research was funded in part by the Scottish Research Partnership in Engineering, in collaboration with The University of Edinburgh and Babcock International Group PLC. All funding sources are hereby gratefully acknowledged. Funding agencies did not have any role in any of the following categories: study design; in the collection, analysis and interpretation of data; in the writing of the article; and in the decision to submit the article for publication.

Data Availability Statement: The data presented in this study are available on request from the corresponding author.

Acknowledgments: The partnership and funding provided by Babcock International Group PLC, in conjunction with the Scottish Research Partnership in Engineering (SRPe) are gratefully acknowledged. The authors would like to thank Jennifer Hughes and Gary Halstead of Babcock International Group PLC for their assistance when scoping this work and their supplying of materials in kind; and extend gratitude to Edward Monteith, University of Edinburgh for his technical wisdom provided throughout this work. The support and cooperation of Sonatest Ltd in providing access (in kind) to the Veo+ ultrasound detector used in this work is gratefully acknowledged. Further thanks are extended to Mike Ennis, David Deeney, and Harry Brittin for their support therein.

Conflicts of Interest: The authors declare no conflict of interest.

Abbreviations

The following abbreviations are used in this manuscript:

NDT	non-destructive testing
RNLI	Royal National Lifeboat Institution
UT	ultrasonic testing
FRP	fibre-reinforced polymer
PAUT	phased array ultrasonic testing
TOFD	time-of-flight diffraction
AUT	automated ultrasonic testing
PTFE	polytetrafluoroethylene
ASTM	ASTM International
FMC	full matrix capture
TFM	total focussing method
CSM	chopped strand mat
EDF	exponential decay function

References

1. Phillips, H. The RNLI's Experiences and Current Application of Marine Composites NDT. In Proceedings of the Marine Composites Inspection Workshop: Sea what you are missing; The British Institute of Non-Destructive Testing: Poole, 2021.
2. Phillips, H. NDE OF COMPOSITE MARINE STRUCTURES. In Proceedings of the New Approaches for Performance Definition of Composite Materials and Structures; British Society of Strain Measurement: London, 2010.
3. Whalley, G.; Queen, N.; Hook, A. Babcock Devenport NDT Composite Overview. In Proceedings of the Marine Composites Inspection Workshop: Sea what you are missing; The British Institute of Non-Destructive Testing: Poole, 2021.
4. Whalley, G.; Hayday, L.; Hook, A. Inspection of naval composites. In Proceedings of the BINDT Workshop 2023: NDT of composites through life; The British Institute of Non-Destructive Testing: Poole, 2023.
5. Taheri, H.; Hassen, A.A. Nondestructive Ultrasonic Inspection of Composite Materials: A Comparative Advantage of Phased Array Ultrasonic. *Applied Sciences* **2019**, *9*, 1628. https://doi.org/10.3390/app9081628.
6. Wang, B.; Zhong, S.; Lee, T.L.; Fancey, K.S.; Mi, J. Non-destructive testing and evaluation of composite materials/structures: A state-of-the-art review. *Advances in Mechanical Engineering* **2014**, *12*, 1–28. https://doi.org/10.1177/1687814020913761.
7. Li, D.; Zhou, J.; Ou, J. Damage, nondestructive evaluation and rehabilitation of FRP composite-RC structure: A review. *Construction and Building Materials* **2021**, *271*, 121551. https://doi.org/10.1016/j.conbuildmat.2020.121551.
8. Qiu, Q. Effect of internal defects on the thermal conductivity of fiber-reinforced polymer (FRP): A numerical study based on micro-CT based computational modeling. *Materials Today Communications* **2023**, *36*, 106446. https://doi.org/https://doi.org/10.1016/j.mtcomm.2023.106446.

9. Duernberger, E.; MacLeod, C.; Lines, D.; Loukas, C.; Vasilev, M. Adaptive optimisation of multi-aperture ultrasonic phased array imaging for increased inspection speeds of wind turbine blade composite panels. *NDT E International* **2022**, *132*, 102725. https://doi.org/https://doi.org/10.1016/j.ndteint.2022.102725.
10. Uhry, C.; Guillet, F.; Duvauchelle, P.; Kaftandjian, V. Optimisation of the process of X-ray tomography applied to the detection of defects in composites materials. In Proceedings of the Digital Industrial Radiology and Computed Tomography; Ghent University, , 2015.
11. Thomas, J.A. HMS Wilton - a glass-reinforced plastics minehunter. *Composites* **1972**, *3*, 79–82. https://doi.org/10.1016/0010-4361(72)90380-1.
12. Hall, D.J.; Robson, B.L. A review of the design and materials evaluation programme for the GRP/foam sandwich composite hull of the RAN minehunter. *Composites* **1984**, *15*, 266–276. https://doi.org/10.1016/0010-4361(84)90707-9.
13. Tran, P.; Wu, C.; Saleh, M.; Bortolan Neto, L.; Nguyen-Xuan, H.; Ferreira, A.J. Composite structures subjected to underwater explosive loadings: A comprehensive review. *Composite Structures* **2021**, *263*, 113684. https://doi.org/10.1016/j.compstruct.2021.113684.
14. Krautkrämer, J.; Krautkrämer, H.; Hislop, J.; Grabendörfer, W.; Frielinghaus, R.; Kaule, W.; Niklas, L.; Opara, U.; Schlengermann, U.; Seiger, H.; et al. *Ultrasonic Testing of Materials*; Springer Berlin Heidelberg, 2013.
15. Automatic Crack Detection and Characterization During Ultrasonic Inspection. *Journal of Nondestructive Evaluation* **2010**, *29*, 169–174. https://doi.org/https://doi.org/10.1007/s10921-010-0074-4.
16. Belyaev, A.; Polupan, O.; Dallas, W.; Ostapenko, S.; Hess, D.; Wohlgemuth, J. Crack detection and analyses using resonance ultrasonic vibrations in full-size crystalline silicon wafers. *Applied Physics Letters* **2006**, *88*, 111907, [https://pubs.aip.org/aip/apl/article-pdf/doi/10.1063/1.2186393/14658014/111907_1_online.pdf]. https://doi.org/10.1063/1.2186393.
17. Yao, Y.; Tung, S.T.E.; Glisic, B. Crack detection and characterization techniques—An overview. *Structural Control and Health Monitoring* **2014**, *21*, 1387–1413, [https://onlinelibrary.wiley.com/doi/pdf/10.1002/stc.1655]. https://doi.org/https://doi.org/10.1002/stc.1655.
18. An, Y.K.; Kwon, Y.; Sohn, H. Noncontact laser ultrasonic crack detection for plates with additional structural complexities. *Structural Health Monitoring* **2013**, *12*, 522–538, [https://doi.org/10.1177/1475921713500515]. https://doi.org/10.1177/1475921713500515.
19. Bahonar, M.; Safizadeh, M.S. Investigation of real delamination detection in composite structure using air-coupled ultrasonic testing. *Composite Structures* **2022**, *280*, 114939. https://doi.org/https://doi.org/10.1016/j.compstruct.2021.114939.
20. Zhang, Z.; Guo, S.; Li, Q.; Cui, F.; Malcolm, A.A.; Su, Z.; Liu, M. Ultrasonic detection and characterization of delamination and rich resin in thick composites with waviness. *Composites Science and Technology* **2020**, *189*, 108016. https://doi.org/https://doi.org/10.1016/j.compscitech.2020.108016.
21. Park, B.; An, Y.K.; Sohn, H. Visualization of hidden delamination and debonding in composites through noncontact laser ultrasonic scanning. *Composites Science and Technology* **2014**, *100*, 10–18. https://doi.org/https://doi.org/10.1016/j.compscitech.2014.05.029.
22. Gao, T.; Wang, Y.; Qing, X. A New Laser Ultrasonic Inspection Method for the Detection of Multiple Delamination Defects. *Materials* **2021**, *14*. https://doi.org/10.3390/ma14092424.
23. Ibrahim, M.E. Ultrasonic inspection of hybrid polymer matrix composites. *Composites Science and Technology* **2021**, *208*, 108755. https://doi.org/https://doi.org/10.1016/j.compscitech.2021.108755.
24. Wu, S.J.; Chin, P.C.; Liu, H. Measurement of Elastic Properties of Brittle Materials by Ultrasonic and Indentation Methods. *Applied Sciences* **2019**, *9*. https://doi.org/10.3390/app9102067.
25. Smith, R.A.; Nelson, L.J.; Mienczakowski, M.J.; Wilcox, P.D. Ultrasonic tracking of ply drops in composite laminates. *AIP Conference Proceedings* **2016**, *1706*, 050006, [https://pubs.aip.org/aip/acp/article-pdf/doi/10.1063/1.4940505/12833566/050006_1_online.pdf]. https://doi.org/10.1063/1.4940505.
26. Yang, X.; Verboven, E.; feng Ju, B.; Kersemans, M. Comparative study of ultrasonic techniques for reconstructing the multilayer structure of composites. *NDT E International* **2021**, *121*, 102460. https://doi.org/https://doi.org/10.1016/j.ndteint.2021.102460.
27. Through transmission ultrasonic inspection of fiber waviness for thickness-tapered composites using ultrasound non-reciprocity: Simulation and experiment. *Ultrasonics* **2022**, *123*, 106716. https://doi.org/https://doi.org/10.1016/j.ultras.2022.106716.
28. Bastianini, F.; Di Tommaso, A.; Pascale, G. Ultrasonic non-destructive assessment of bonding defects in composite structural strengthenings. *Composite Structures* **2001**, *53*, 463–467. https://doi.org/https://doi.org/10.1016/S0263-8223(01)00058-7.
29. Daniel, I.M.; Wooh, S.C., Ultrasonic Techniques for Characterization of Manufacturing Defects in Thick Composites. In *Review of Progress in Quantitative Nondestructive Evaluation: Volume 8, Part A and B*; Thompson, D.O.; Chimenti, D.E., Eds.; Springer US: Boston, MA, 1989; pp. 1605–1612. https://doi.org/10.1007/978-1-4613-0817-1_202.
30. Kokurov, A.M.; Subbotin, D.E. Ultrasonic detection of manufacturing defects in multilayer composite structures. *IOP Conference Series: Materials Science and Engineering* **2021**, *1023*, 012013. https://doi.org/10.1088/1757-899X/1023/1/012013.
31. Cao, A.; Li, Q.; Yang, W.; Zhang, Z. Frequency shifting of transmitted ultrasound in thick composites containing fiber wrinkles and its application in non-destructive evaluation. *Composite Structures* **2023**, *314*, 116939. https://doi.org/https://doi.org/10.1016/j.compstruct.2023.116939.

32. Inês Silva, M.; Malitckii, E.; Santos, T.G.; Vilaça, P. Review of conventional and advanced non-destructive testing techniques for detection and characterization of small-scale defects. *Progress in Materials Science* **2023**, *138*, 101155. https://doi.org/https://doi.org/10.1016/j.pmatsci.2023.101155.
33. Opačić, M.; Sedmak, A.; Bakić, G.; Milošević, N.; Milovanovic, N. Application of advanced NDT methods to assess structural integrity of pressure vessel welded joints. *Procedia Structural Integrity* **2022**, *42*, 1185–1189. 23 European Conference on Fracture, https://doi.org/https://doi.org/10.1016/j.prostr.2022.12.151.
34. Rodriguez, A.G.; Gosselin, A.; Rhéaume, R.; Harrap, N. Computational intelligence approaches for data analysis, the next step of innovation for advanced UT techniques in NDT. In Proceedings of the ECNDT 2018 - 12th European Conference on Non-Destructive Testing (ECNDT 2018), Gothenburg 2018, June 11-15; e-Journal of Nondestructive Testing (eJNDT): Gothenburg, 2018.
35. Yılmaz, B.; Jasiūnienė, E. Advanced ultrasonic NDT for weak bond detection in composite-adhesive bonded structures. *International Journal of Adhesion and Adhesives* **2020**, *102*, 102675. https://doi.org/https://doi.org/10.1016/j.ijadhadh.2020.102675.
36. Segreto, T.; Bottillo, A.; Teti, R. Advanced Ultrasonic Non-destructive Evaluation for Metrological Analysis and Quality Assessment of Impact Damaged Non-crimp Fabric Composites. *Procedia CIRP* **2016**, *41*, 1055–1060. Research and Innovation in Manufacturing: Key Enabling Technologies for the Factories of the Future - Proceedings of the 48th CIRP Conference on Manufacturing Systems, https://doi.org/https://doi.org/10.1016/j.procir.2015.12.125.
37. Revel, G.M.; Pandarese, G.; Cavuto, A. Advanced ultrasonic non-destructive testing for damage detection on thick and curved composite elements for constructions. *Journal of Sandwich Structures & Materials* **2013**, *15*, 5–24. https://doi.org/10.1177/1099636212456861.
38. Lupien, V. Principles of Phased Array Ultrasound for Nondestructive Testing. *Materials Evaluation* **2007**, *65*.
39. TOWSYFYAN, H.; BIGURI, A.; BOARDMAN, R.; BLUMENSATH, T. Successes and challenges in non-destructive testing of aircraft composite structures. *Chinese Journal of Aeronautics* **2020**, *33*, 771–791. https://doi.org/https://doi.org/10.1016/j.cja.2019.09.017.
40. Brizuela, J.; Camacho, J.; Cosarinsky, G.; Iriarte, J.; Cruza, J. Improving elevation resolution in phased-array inspections for NDT. *NDT E International* **2019**, *101*, 1–16. https://doi.org/https://doi.org/10.1016/j.ndteint.2018.09.002.
41. Zobeiry, N.; Bayat, S.; Anas, E.; Mousavi, P.; Abolmaesumi, P.; Poursartip, A. Temporal Enhanced Ultrasound As A Novel NDT Technique For Defects In Composites. In Proceedings of the Proceedings of the American Society for Composites Thirty-Third Technical Conference. Proceedings of the 18th US-Japan Conference on Composite Materials ATSM Committee D30 Meeting; The American Society for Composites: SEATTLE, WASHINGTON, 2018. https://doi.org/10.12783/asc33/26149.
42. Hsu, D.K.; Jeong, H., Ultrasonic Velocity Change and Dispersion Due to Porosity in Composite Laminates. In *Review of Progress in Quantitative Nondestructive Evaluation: Volume 8, Part A and B*; Thompson, D.O.; Chimenti, D.E., Eds.; Springer US: Boston, MA, 1989; pp. 1567–1573. https://doi.org/10.1007/978-1-4613-0817-1_197.
43. Ishii, Y.; Biwa, S.; Kuraishi, A. Influence of porosity on ultrasonic wave velocity, attenuation and interlaminar interface echoes in composite laminates: Finite element simulations and measurements. *Composite Structures* **2016**, *152*, 645–653. https://doi.org/https://doi.org/10.1016/j.compstruct.2016.05.054.
44. Kapadia, A., Best Practice Guide Non-Destructive Testing of Composite Materials; National Composites Network, 2013.
45. Hsu, D.K.; Minachi, A., Defect Characterization in Thick Composites by Ultrasound. In *Review of Progress in Quantitative Nondestructive Evaluation*; Thompson, D.O.; Chimenti, D.E., Eds.; Springer US: Boston, MA, 1990; pp. 1481–1488. https://doi.org/10.1007/978-1-4684-5772-8_190.
46. Mouritz, A.P. Ultrasonic and Interlaminar Properties of Highly Porous Composites. *Journal of Composite Materials* **2000**, *34*, 218–239, [https://doi.org/10.1177/002199830003400303]. https://doi.org/10.1177/002199830003400303.
47. Kersemans, M.; Verboven, E.; Segers, J.; Hedayatrasa, S.; Paepegem, W.V. Non-Destructive Testing of Composites by Ultrasound, Local Defect Resonance and Thermography. *Proceedings* **2018**, *2*. https://doi.org/10.3390/ICEM18-05464.
48. Mouritz, A.P.; Townsend, C.; Shah Khan, M.Z. Non-destructive detection of fatigue damage in thick composites by pulse-echo ultrasonics. *Composites Science and Technology* **2000**, *60*, 23–32.
49. Drinkwater, B.W.; Wilcox, P.D. Ultrasonic arrays for non-destructive evaluation: A review. *NDT and E International* **2006**, *39*, 525–541. https://doi.org/10.1016/j.ndteint.2006.03.006.
50. Nsengiyumva, W.; Zhong, S.; Lin, J.; Zhang, Q.; Zhong, J.; Huang, Y. Advances, limitations and prospects of nondestructive testing and evaluation of thick composites and sandwich structures: A state-of-the-art review. *Composite Structures* **2021**, *256*. https://doi.org/10.1016/j.compstruct.2020.112951.
51. Battley, M.; Skeates, A.; Simpkin, R.; Holmqvist, A. Non-Destructive Inspection of Marine Composite Structures. In Proceedings of the High Performace Yacht Design Conference; , 2002.
52. Balasubramaniam, K.; Whitney, S.C. Ultrasonic through-transmission characterization of thick fibre-reinforced composites. *NDT & E International* **1996**, *29*, 225–236. https://doi.org/10.1016/S0963-8695(96)00014-X.
53. Ibrahim, M.E. Nondestructive evaluation of thick-section composites and sandwich structures: A review. *Composites Part A: Applied Science and Manufacturing* **2014**, *64*, 36–48. https://doi.org/10.1016/j.compositesa.2014.04.010.
54. Ibrahim, M.E. Nondestructive testing and structural health monitoring of marine composite structures. In *Marine Applications of Advanced Fibre-Reinforced Composites*; Elsevier Inc., 2016; pp. 147–183. https://doi.org/10.1016/B978-1-78242-250-1.00007-7.
55. Sheppard, P.J.; Phillips, H.J.; Cooper, I. The practical use of NDE methods for the assessment of damaged marine composite structures. *ICCM International Conferences on Composite Materials* **2009**.

56. Davidson, J.R.; Quinn, J.A.; Rothmann, C.; Bajpai, A.; Robert, C.; Ó Brádaigh, C.M.; McCarthy, E.D. Mechanical characterisation of pneumatically-spliced carbon fibre yarns as reinforcements for polymer composites. *Materials & Design* **2022**, *213*, 110305. https://doi.org/10.1016/j.matdes.2021.110305.
57. Obande, W.; Stankovic, D.; Bajpai, A.; Devine, M.; Wurzer, C.; Lykkeberg, A.; Garden, J.A.; Ó Brádaigh, C.M.; Ray, D. Thermal reshaping as a route for reuse of end-of-life glass fibre-reinforced acrylic composites. *Composites Part B: Engineering* **2023**, *257*, 110662. https://doi.org/10.1016/j.compositesb.2023.110662.
58. Khalid, M.Y.; Arif, Z.U.; Ahmed, W.; Arshad, H. Recent trends in recycling and reusing techniques of different plastic polymers and their composite materials. *Sustainable Materials and Technologies* **2022**, *31*, e00382. https://doi.org/10.1016/j.susmat.2021.e00382.
59. O'Rourke, K.; Wurzer, C.; Murray, J.; Doyle, A.; Doyle, K.; Griffin, C.; Christensen, B.; Ó Brádaigh, C.M.; Ray, D. Diverted from Landfill: Reuse of Single-Use Plastic Packaging Waste. *Polymers* **2022**, *14*. https://doi.org/10.3390/polym14245485.
60. Bond, L.J.; Ahmad, A. Fundamentals Ultrasonic Inspection. *ASM Handbook, Nondestructive Evaluation of Materials* **2018**, *17*, 698.